FISEVIER

Contents lists available at ScienceDirect

Electric Power Systems Research

journal homepage: www.elsevier.com/locate/epsr



Physics-based analytical model for high impedance fault location in distribution networks



Maicon J.S. Ramos*,^a, Mariana Resener^a, Arturo S. Bretas^c, Daniel P. Bernardon^b, Roberto C. Leborgne^a

- ^a Universidade Federal do Rio Grande do Sul, Porto Alegre, RS, Brazil
- Universidade Federal de Santa Maria, Santa Maria, RS, Brazil
- ^c University of Florida, Gainesville, FL, USA

ARTICLE INFO

Keywords: High impedance fault location Power distribution systems Power distribution protection Frequency domain analysis

ABSTRACT

This paper presents a physics-based analytical model for high impedance fault location in power distribution systems. The presented analytical solution is composed by two interdependent processes. First, fault distance is estimated through a Weighted Least Square approach applied to solve an overdetermined and nonlinear algebraic system of equations. Second, an analytical method based on the statistical behavior of the estimates obtained from the frequency domain system model solution is presented to address the multiple estimates problem, identifying the faulted section. The presented fault location physics-based analytical model considers the capacitive effect of distribution lines. Furthermore, voltages and currents measured from only one terminal are used. The formulation is evaluated using the IEEE 13-bus and a modified version of the IEEE 34-bus test feeders. Comparative analysis with state-of-the-art methods is presented. Average errors of 1.95% are obtained. Easy to implement analytical model, without hard to derive parameters, built on the weighted least squares state estimator, highlight potential aspects for real-life applications.

1. Introduction

Power distribution systems (PDS) composed of overhead distribution lines (ODL) are greatly exposed to the most diverse types of faults due to their constructive characteristics. Faults are a stochastic phenomena that affect the system operation and are mainly caused by atmospheric discharges, tree contact and connection issues [1].

Many studies have presented statistical data observing that between 70% and 90% of faults recorded in ODL are non permanent and involve an electric arc [2,3]. As presented in [2], 90% of these faults are phase-to-ground and can be eliminated by the actuation of circuit breakers or automatic reclosers. Electric arc formation at the fault location is one of the characteristics of a high impedance fault (HIF) and is the result of the poor contact between ground and the conductor [4]. According to Jeerings and Linders [4], Emanuel et al. [5], a HIF fault is characterized by a build-up time period, where the amplitude of the fault current increases, reaching its maximum value after a few cycles, and a shoulder period, where the fault current remains stable during few cycles within the build-up time period.

Several methods for fault location in PDS have been proposed over the last decades. The majority of these works are based on the apparent impedance and consider a purely constant resistive fault (linear characteristic) model, as in [6-12]. These works present accurate estimates of the fault location and consider the inherent characteristics of distribution networks.

On the other hand, analytical approaches for locating HIF in PDS considering a more realistic fault model are seldom in the literature. HIF modeling involves the representation of the electric arc at the fault point [5,13], and its detection and location on distribution networks are very challenging [14–18]. This is because of the physics characteristics of a HIF, such as: fault current with small magnitude, presence of harmonic currents and nonlinear behavior [5].

Considering HIF location, [19] presents a time-domain physics-based system model. State variables are estimated through a least squares approach and Newton's Method. A linear least square estimator is initially applied, not considering the line capacitance for system model derivation. After, a state estimator based on a steepest descent approach is applied considering the line capacitance effect. Tests were carried out for the 13 bus system of IEEE.

In [20], a frequency domain system model for HIF location is solved through a Weighted Least Squares (WLS) parameter estimation approach. The formulation considers the line capacitive effect, arc

E-mail address: maicon.jaderson@ufrgs.br (M.J.S. Ramos).

^{*} Corresponding author.

resistance, and inherent unbalanced distribution systems operation. However, when applied to a feeder with branch laterals, multiple estimates arise and the identification of the faulted section is not addressed.

Recently, a HIF location analytical model was presented in [21], in which a neural network is used to estimate the parameters of the feeder during the fault period. The fault distance is estimated considering a time-domain system model, which includes derivatives estimated through a polynomial approximation approach. In addition, the model parameters are estimated considering the shoulder period, when the fault current is constant. Regarding the time-domain system model, the method considers the entire load of the feeder concentrated downstream of the fault point, which is a strong assumption when the feeder has branch laterals. Thus, important estimation errors are obtained for faults applied in lateral branches.

The HIF location was addressed recently in [22], where a spectral domain formulation is presented. In this approach, an algorithm is used to detect the presence of parameter errors related to the distortions associated with HIF currents and then correct the model. Tests were carried out in the IEEE 13-node test feeder, showing great advances in the HIF location problem. However, the faulted section identification is not addressed.

Frequency domain physics-based system models present some advantages over time domain ones. For a steady state condition, an algebraic set of equations can be derived and the state estimation process is easier to implement numerically when compared to a set of differential equations in time domain. Methods for HIF location modeled in the frequency domain were proposed in [3,11,15,23]. These methods consider balanced system and the line capacitance is not modeled. In addition, the parameters of the system during a fault are estimated only during the shoulder HIF period and the formulations require measures from more than one location.

In this work, an analytical physics-based system model for HIF location and section identification is presented and discussed. The analytical model is composed of two interdependent processes. First, the HIF location is estimated considering a frequency domain system model solved by a WLS state estimator based on [20]. The faulted system model considers the inherent characteristics of a distribution feeder and the line capacitance effect, and the HIF is modeled by two antiparallel diodes and an arc resistance [5,20,23]. Second, a novel methodology to estimate the faulted section identification based on the analysis of the statistical behavior of the estimates is proposed. It is most important to highlight that the faulted section identification is not addressed in [20]. Thus, the presented analytical model can be considered as a contribution towards comprehensive solutions for HIF location in PDS.

The main contributions of this work are:

- a methodology to perform the section identification based on the analysis of the statistical behavior of the estimates, in order to eliminate multiple estimates when the feeder has branch laterals, differing from Ramos et al. [20], Nunes et al. [22];
- a comprehensive approach for HIF location in PDS considering a frequency domain system model, differing from the time-domain system models presented in [19,21].

The remainder of this paper is organized as follows. Section II presents the analytical model for HIF location in distribution systems. Section III presents the faulted section identification analytical model, and Section IV presents comparative test results considering the IEEE 13-bus test system and a modified version of the IEEE 34-bus test system. Finally, Section V presents the conclusions of this work.

2. HIF Location methodology

In this work, the formulation derivation for HIF location in PDS is based on the frequency domain system model presented in [20].

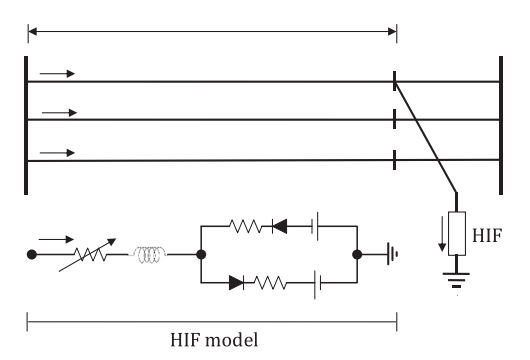


Fig. 1. Model of the system and HIF [20].

According to Radojevic [23], the voltage at the fault can be modeled by an arc voltage in series with an arc resistance and represented by the sum of the multiple harmonics components; however, the author states that the harmonics above the third order can be neglected, since they have comparative low magnitudes. We use the model proposed in [11] to represent a HIF, which is composed by two antiparallel diodes and an arc impedance, as shown in Fig. 1.

Consider a line section with a HIF on phase A located at *y* km from the sending end bus, illustrated in Fig. 1.

Analyzing the circuit of the fault model in Fig. 1, the *h*th harmonic of the fault voltage can be defined as:

$$V_{Fh_a} = (R_{Fa} + jX_{Fa}) \cdot I_{Fh_a} \tag{1}$$

where $R_{Fa} = (R_F + R_a)$, R_F is the fault resistance, R_a is the arc resistance, X_{Fa} is the fault reactance, V_{Fh} and I_{Fh} are the hth harmonic of the voltage and current at the fault, respectively.

Through the analysis of the system in Fig. 1, it is possible to obtain [24]:

$$\begin{bmatrix} V_F \\ I_F \end{bmatrix} = \begin{bmatrix} d_y & -b_y \\ -c_y & a_y \end{bmatrix} \cdot \begin{bmatrix} V_s \\ I_s \end{bmatrix}$$
 (2)

where a_y , b_y , c_y and d_y are defined by:

$$a_y = d_y = I + 0.5 \cdot y^2 \cdot Z_{abc} \cdot Y_{abc}$$
(3)

$$b_{y} = y \cdot Z_{abc}, \tag{4}$$

$$c_y = y \cdot Y_{abc} + 0.25 \cdot y^3 \cdot Y_{abc} \cdot Z_{abc} \cdot Y_{abc}$$
 (5

and where V_F and V_s represent, respectively, the three-phase voltages phasors at the faulted bus and sending end bus, while I_F and I_s represent the three-phase current phasors at the faulted bus and the sending end bus, respectively. I is the identity matrix, Z_{abc} is the line series impedance matrix in $[\Omega/km]$, and Y_{abc} is the line shunt admittance matrix in [S/km].

From Eqs. (1) and (2), one can obtain:

$$(R_{Fa} + jX_{Fa}) \cdot I_{Fh} = d_y \cdot V_{sh} - b_y \cdot I_{sh}, \tag{6}$$

where V_{sh} is the harmonic h of the voltage at the sending end bus, I_{sh} is the harmonic h of the current at the sending end bus, and I_{Fh} is the harmonic h of the fault current.

Using (3) and (4), Eq. (6) can be rewritten for each phase k as:

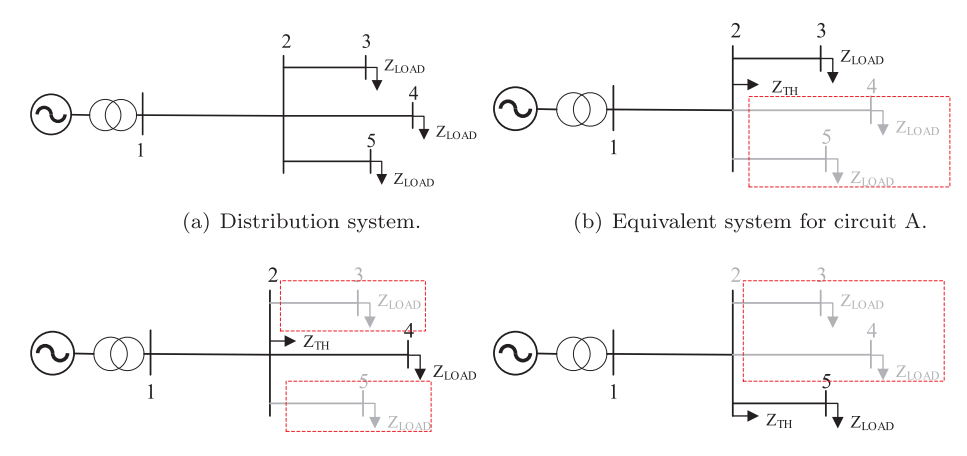
$$V_{sh_k} = (R_{Fa} + jX_{Fa}) \cdot I_{Fh_k} + y \cdot M_{h_k} - 0.5 \cdot y^2 \cdot N_{h_k}, \tag{7}$$

where:

 V_{sh_k} hth harmonic of the voltage at the sending end bus on phase k [V];

 I_{sh_k} hth harmonic of the current at the sending end bus on phase k [A];

I_{Fhk} hth harmonic of the fault current on phase k [A]; y estimated fault distance [km];



(c) Equivalent system for circuit B.

(d) Equivalent system for circuit C.

Fig. 2. Distribution system with lateral branches and equivalent systems.

and:

$$\begin{bmatrix} M_{h_a} \\ M_{h_b} \\ M_{h_c} \end{bmatrix} = \begin{bmatrix} Z_{h_{aa}} & Z_{h_{ab}} & Z_{h_{ac}} \\ Z_{h_{ba}} & Z_{h_{bb}} & Z_{h_{bc}} \\ Z_{h_{ca}} & Z_{h_{cb}} & Z_{h_{cc}} \end{bmatrix} \cdot \begin{bmatrix} I_{sh_a} \\ I_{sh_b} \\ I_{sh_c} \end{bmatrix},$$

$$\begin{bmatrix} I_{sh_a} \\ I_{sh_b} \\ I_{sh_c} \end{bmatrix},$$

$$(8)$$

$$\begin{bmatrix} N_{h_a} \\ N_{h_b} \\ N_{h_c} \end{bmatrix} = \begin{bmatrix} Z_{h_{aa}} & Z_{h_{ab}} & Z_{h_{ac}} \\ Z_{h_{ba}} & Z_{h_{bb}} & Z_{h_{bc}} \\ Z_{h_{ca}} & Z_{h_{cb}} & Z_{h_{cc}} \end{bmatrix} \cdot \begin{bmatrix} Y_{h_{aa}} & Y_{h_{ab}} & Y_{h_{ac}} \\ Y_{h_{ba}} & Y_{h_{bb}} & Y_{h_{bc}} \\ Y_{h_{ca}} & Y_{h_{cb}} & Y_{h_{cc}} \end{bmatrix} \cdot \begin{bmatrix} V_{sh_a} \\ V_{sh_b} \\ V_{sh_c} \end{bmatrix}.$$
(9)

where $Z_{h_{kk}}$ and $Y_{h_{kk}}$ are the hth harmonic component of the self-impedance and self-admittance of phase k. Furthermore, $Z_{h_{kj}}$ and $Y_{h_{kj}}$ are the hth harmonic component of the mutual impedance and admittance between phases k and j.

Considering a fault on phase a and writing (7) considering its real (r) and imaginary (i) components, an undetermined set of nonlinear equations is obtained:

$$\begin{bmatrix} V_{sh_a}^r \\ V_{sh_a}^i \end{bmatrix} = \begin{bmatrix} I_{Fh_a}^r & -I_{Fh_a}^i & M_{h_a}^r & -0.5 \cdot N_{h_a}^r \\ I_{Fh_a}^i & I_{Fh_a}^r & M_{h_a}^i & -0.5 \cdot N_{h_a}^i \end{bmatrix} \cdot \begin{bmatrix} R_{Fa} \\ X_{Fh_a} \\ y \\ y^2 \end{bmatrix}$$
(10)

The undetermined set of Eq. (10) can be transformed in an overdetermined one through the consecutive phasors obtained applying the sliding window concept proposed in [20]. The overdetermined set of equations is defined as:

$$\begin{bmatrix} V_{sh_{a1}}^{r} \\ V_{sh_{a1}}^{r} \\ V_{sh_{a1}}^{r} \\ V_{sh_{a2}}^{r} \\ V_{sh_{a2}}^{r} \\ \vdots \\ V_{sh_{an}}^{r} \\ V_{sh_{an}}^{r} \end{bmatrix} = \begin{bmatrix} I_{Fh_{a1}}^{r} & -I_{Fh_{a1}}^{i} & M_{h_{a1}}^{r} & -0.5 \cdot N_{h_{a1}}^{r} \\ I_{Fh_{a1}}^{r} & I_{Fh_{a1}}^{r} & M_{h_{a1}}^{r} & -0.5 \cdot N_{h_{a1}}^{r} \\ I_{Fh_{a2}}^{r} & -I_{Fh_{a2}}^{r} & M_{h_{a2}}^{r} & -0.5 \cdot N_{h_{a2}}^{r} \\ I_{Fh_{a2}}^{r} & I_{Fh_{a2}}^{r} & M_{h_{a2}}^{r} & -0.5 \cdot N_{h_{a2}}^{r} \\ \vdots & \vdots & \vdots & \vdots \\ I_{Fh_{an}}^{r} & -I_{Fh_{an}}^{r} & M_{h_{an}}^{r} & -0.5 \cdot N_{h_{an}}^{r} \\ V_{sh_{an}}^{r} \end{bmatrix} \cdot \begin{bmatrix} R_{Fa} \\ X_{Fh_{a1}}^{r} \\ Y \\ Y^{2} \end{bmatrix}$$

where the subscripts $(1, 2, \cdots, n)$ are the consecutive estimated phasors. The Weighted Least Squares (WLS) state estimator (SE) and the Newton-Raphson method [25] are applied to solve the system of equations presented in (11). In this work the faulty phase identification is considered known.

The fault current estimation is made considering the solution proposed in [9]. An initial fault current estimate is obtained by the difference between currents measured during and before the fault occurrence at the substation bus. Then, a new fault distance estimate is obtained through (11) and a new fault current can be determined using (6). This iterative process is repeated until a convergence criteria is

satisfied.

2.1. Fault parameter estimation

Using phasors to estimate the fault parameters can result in inaccurate estimates, since the HIF parameters vary considerably during the fault period. In order to overcome this, we apply a residual analysis [20]. In this method, a binary control variable (BCV) is defined to select the best estimates for the WLS SE.

During the fault period, numerous samples of voltage and current signals are recorded, and estimates of the fault parameters are made for the entire set of recorded samples. As the sliding window moves to capture new phasors, a new set of equations is used to estimate the fault parameters. Thus, a set of estimates with corresponding residuals results. Using this set of estimates with corresponding residuals, we obtain the mean value of residuals.

Estimates with residuals higher than 3 standard deviations are not considered [26], thus the BCV is equal to zero in these cases. Otherwise, the BCV will be equal to one and the estimate is considered. A modified Fourier Transform Filter [27] is used to estimate the phasors.

3. Faulted section identification

In order to eliminate multiple estimates and identify the correct physical fault location, equivalent circuits of the distribution feeder for each lateral branch are modeled [9]. Initially, possible power flow paths are identified and, in order to obtain the equivalent systems, lines and loads outside the path being analyzed are transformed into equivalent constant impedances along the radial system. Loads are represented as constant impedances and other load models are considered out of the scope of the paper. The model presented in Section 2 is applied to each equivalent system to estimate the parameters of the fault and then a set of fault location estimates based on the phasors from the voltage and current signals is obtained. The question that begs an answer is then which one of these estimates corresponds to the correct physical fault location?

In order to present the fault section identification method, consider the distribution feeder with three lateral branches as presented in Fig. 2(a). This system has a main feeder trunk, which is the line section between the bus 1 and 2, and three lateral branches connected to bus 2. Thus, three equivalent circuits can be obtained, as illustrated in Figs. 2(b)–(d). The two remaining lateral branches are represented by an equivalent impedance (Z_{TH}) every time an equivalent circuit is obtained.

After, when the WLS SE is applied to the equivalent circuits, we theorize that, due to the existing variability in the HIF parameters, only

the correct equivalent circuit will present a stable statistical characteristic. Stable statistical characteristic is defined here as quasi steady state statistical characteristic of the fault location estimates. This assumption is most reasonable, since equivalent circuits not containing the HIF line section will show a purposeful additive model error. One set of fault distance estimates for each equivalent circuit is then obtained. The size of the set will depend on the number of voltage and current signal samples considered.

Considering the three lateral branches and the main feeder trunk of the feeder illustrated in Fig. 2(a), the sets of solutions will then present different statistical characteristics depending on the physically correct fault location and on the electrical characteristics of the lateral branches. We can expect two different statistical characteristics of the fault location estimates considering faults on sections belonging to the main feeder trunk and faults on lateral branches.

3.1. Faults on the main feeder trunk

Considering the system in Fig. 2(a), it is verified that a fault in the section from bus 1 to bus 2 will be common to the three circuits presented in Fig. 2(b)–(d). Therefore, the expected statistical characteristic of the fault location estimates for the three circuits must be the similar. In order to illustrate such, faults were applied in the section between bus 1 and 2. The fault distance estimates and fitted lines for the three circuits are presented in Fig. 3, where the boxes contain the equations of the fitted lines and the corresponding R-squared (R^2) . The equations of the fitted lines are obtained with linear regression of the estimates of the fault distance (y) and the estimate number (x) [28].

The R-squared statistic will be used as a metric for how horizontal the fitted line is. If this metric is high, this means that the fitted line is not much horizontal, otherwise the fitted line is and thus the fault is on the analyzed line section.

From Fig. 3, one can see that the variability in the estimates is practically null and that the slopes of the fitted lines are very small. Then, the fault distance is approximately 0.4 km (average of the estimated fault distances of each circuit) from the substation bus, which is a point common to the three circuits.

3.2. Faults on the lateral branches

Consider now a HIF on phase A of the line connecting bus 2 to bus 3 (see Fig. 2(a)), which is part of the equivalent circuit A. The statistics of the estimates for the three equivalent circuits is presented in Fig. 4, where the fitted lines and corresponding \mathbb{R}^2 values are shown.

From Fig. 4 one can verify the low variability of the estimates in circuit A, which contains the lateral branch in fault. Furthermore, when

compared to the estimates variabilities derived considering circuits B and C, the variability in circuit A is negligible. Then, the fault is located in circuit A, at approximately 1.7 km from the substation bus.

HIFs were also applied on phase A of line sections connecting bus 2 to bus 4 (circuit B) and bus 2 to bus 5 (circuit C). Test results are presented in Figs. 5 and 6, respectively. From Fig. 5, it is possible to observe the lower variability in the estimates of circuit B, which contains the line section under fault, compared to circuits A and C; then, the fault is located in the circuit B at a point 1.4 km from the substation bus. On the other hand, Fig. 6 shows a lower variability in circuit C, which contains the faulted section; in this case, the estimated fault distance results in 1.35 km from the substation bus. in circuit C.

3.3. Fault section identification

The fault section identification presented in this work is based on the \mathbb{R}^2 values of the fitted lines obtained with linear regression of the estimates of the fault distance. When a high \mathbb{R}^2 is observed, a high variability in the estimates is found. This is associated with the variation of the parameters of a HIF and the additive error imposed to the model when estimating the fault location using an equivalent circuit not containing the fault [29]. On the other hand, when the evaluation is performed using the correct circuit, the fault estimates statistics remain practically constant, even with the variation of the HIF parameters.

In order to identify the lateral branch where the fault is located, we use the R^2 information. The correct lateral branch will be the one with the smallest R^2 value, since this represents almost no variability in the estimates. This can be observed in the examples presented in Figs. 4–6, where the equivalent circuit containing the lateral branch under fault presented the lowest R^2 value.

When the fault is at the main feeder trunk, the \mathbb{R}^2 values will be low for all the equivalent circuits, which was observed in the example presented in Fig. 3. In this case, a tolerance in the difference between the \mathbb{R}^2 values for each equivalent circuit is adopted. Based on observation, the absolute difference should not exceed 0.1 to consider that the fault is at the main feeder trunk. This value was determined empirically and has demonstrated to be a good criterion in all the tests performed to validate the proposed methodology. For different networks, we recommend a sensitivity test to evaluate this parameter.

4. Numerical results

In order to validate the proposed methodology, two test systems were used: the 13-bus [21] and the IEEE 34-bus system [30]. High impedance faults were simulated using the ATP-EMTP and the algorithm was implemented in MATLAB. The fault model considers the

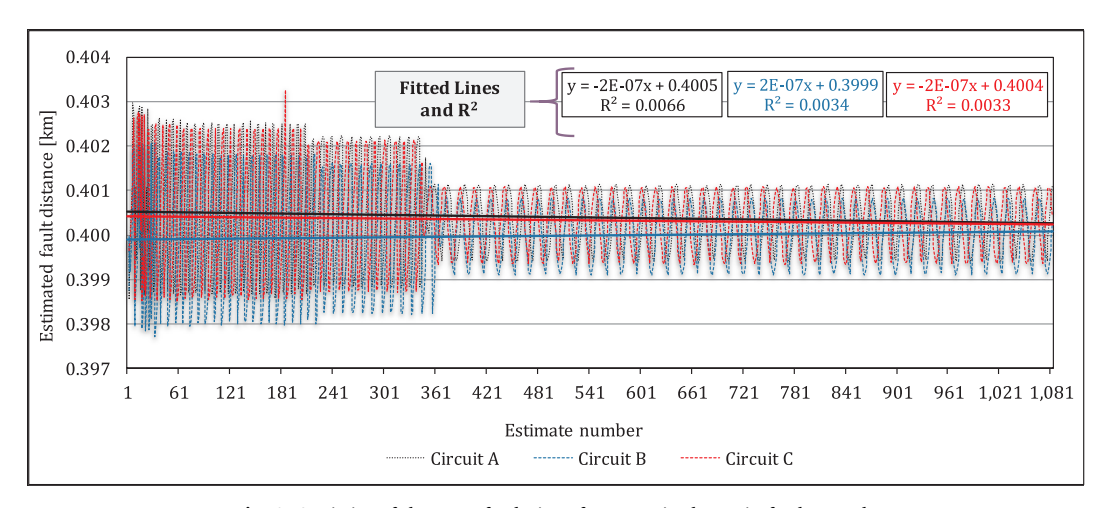


Fig. 3. Statistics of the sets of solutions for a HIF in the main feeder trunk.

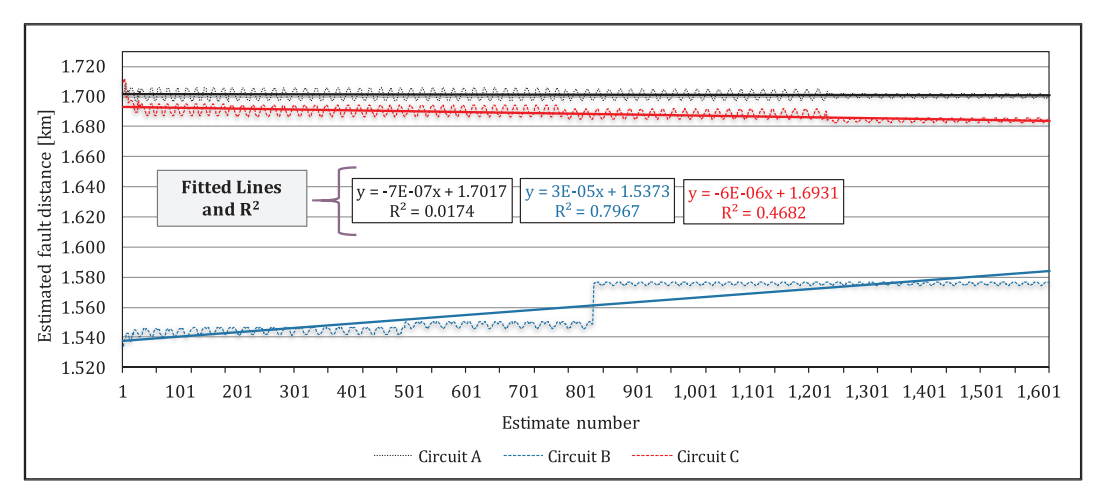


Fig. 4. Statistics of the sets of solutions considering a HIF in circuit A.

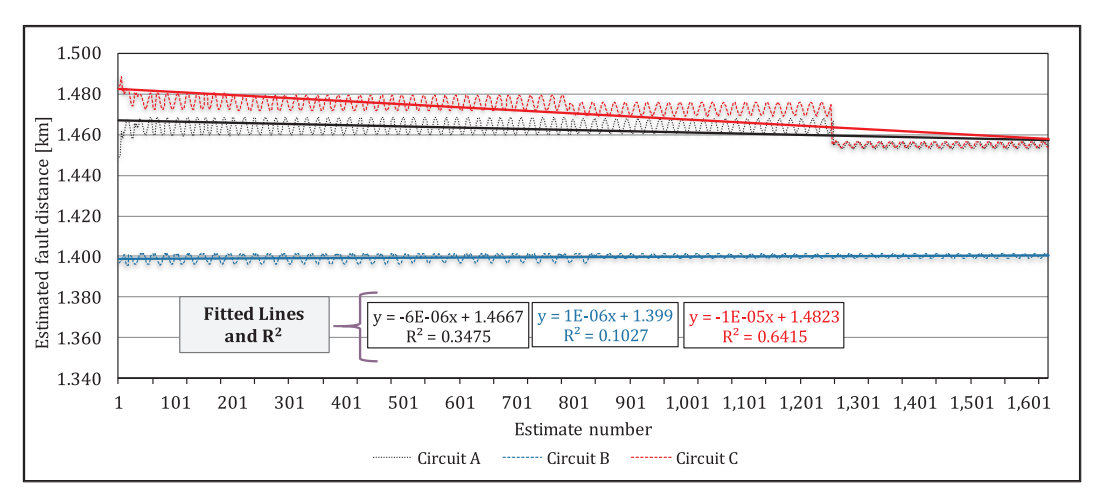


Fig. 5. Statistics of the sets of solutions considering a HIF in circuit B.

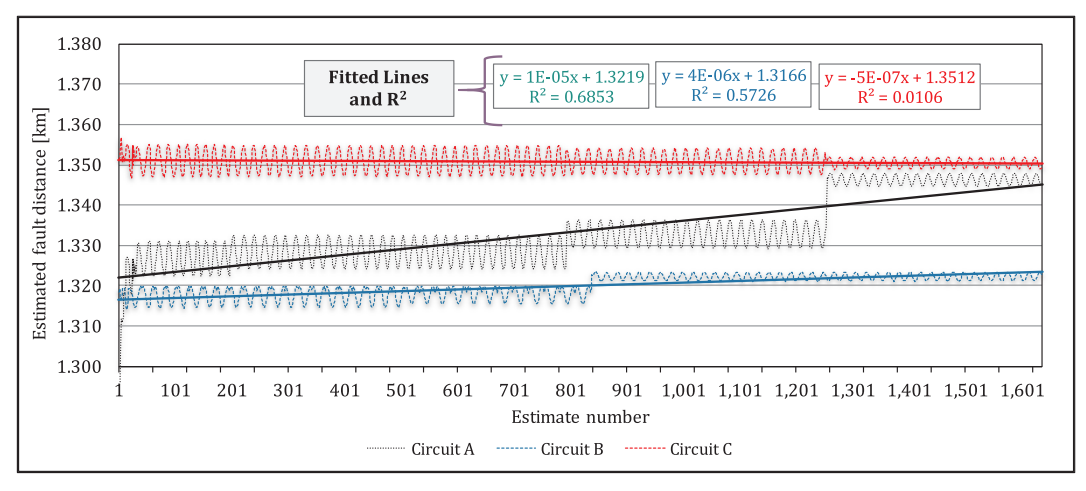


Fig. 6. Statistics of the sets of solutions considering a HIF in circuit C.

build-up and shoulder effects, using a fault resistance which varies with time, as shown in Fig. 7. Furthermore, a reactance with constant value equal to 0.1Ω was considered in the fault impedance model.

The performance of the proposed method was evaluated using the percentage error in the estimated fault distance (y_{est}) defined as follows:

$$error[\%] = 100 \cdot \left| \frac{y_{sim}[km] - y_{est}[km]}{\ell_{line}[km]} \right|$$
(12)

where ℓ_{line} represents the length of the feeder, and y_{sim} represents the distance of the fault from the substation bus.

4.1. 13-Bus system

Data of the 13-bus system [21] was used to compare the results of the presented methodology with the results obtained using the methods presented in [19] and [21]. Faults were applied on phase A of all buses

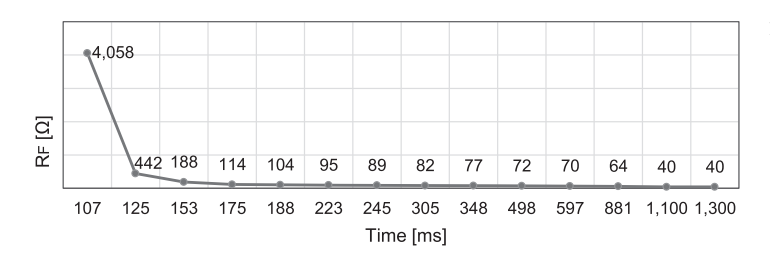


Fig. 7. Fault resistance parameters, adapted from Ferraz et al. [11].

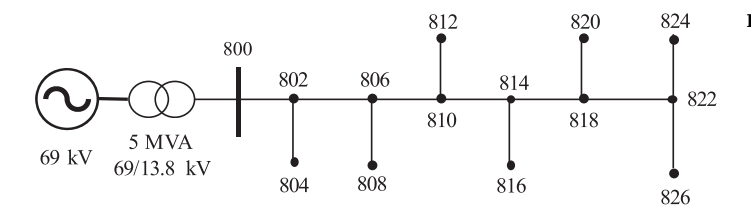


Fig. 8. 13-bus system.

and initially it was assumed that the faulted section is known, comparing the fault distance results. The 13-bus system is illustrated in Fig. 8.

Table 1 presents the results obtained with the presented methodology and using the methods described in [19] and [21]. From these results, a good performance of the method presented can be observed, with errors lower than the other methods for most of the cases.

According to Table 1, a similar performance was observed between the proposed method and [21]. The highest average error found in [21] is 1.60% for a fault at the bus 826, while in the proposed method the highest average error was 1.678%. It is most important to highlight that the method presented in [21] considers a time-domain system model and uses a neural network to estimate the parameters of the feeder during the fault period. On the other hand, in the proposed method the HIF location is estimated considering a frequency domain system model. According to Phadke and Thorp [31] and Dugan et al. [32], frequency domain methods are simpler to implement in real system application when compared to other alternatives. This is mainly due to equation simplicity and user friendly parameter setting.

4.2. 34-Bus system

In this set of test cases, a modified version of the IEEE 34-bus system [30] was considered. The following simplifications were made: (i) the voltage regulators originally in branches 814–850 and 852-832 were not modeled; (ii) the network downstream of the branch 832–888, which includes a transformer and a 4.16 kV network, was modeled as an equivalent load at the bus 832. Loads were represented considering a constant impedance behavior. Load and line data are found in [30]. The substation transformer connection is $\Delta - Y_g$ and it operates at 115/24.9 kV, with a total impedance equal to 0.01 + j0.08 pu. As this system has eight lateral branches, eight equivalent systems are determined,

 Table 1

 Comparative analysis - average errors.

Bus	km from substation	Proposed	[21]	[19]
802	3.0	0.3030%	0.3200%	0.3850%
804	5.0	0.4553%	0.8750%	1.1200%
806	6.0	0.6556%	1.0000%	1.4500%
810	7.0	0.7545%	0.7700%	1.0000%
812	9.0	0.8557%	1.2250%	2.0000%
814	9.5	1.0369%	0.7550%	3.0000%
818	10	1.0526%	1.3750%	4.0000%
820	11	1.1360%	1.3000%	4.2000%
822	12	1.3177%	1.2200%	3.7000%
824	13	1.3261%	1.4700%	4.3000%
826	15	1.6782%	1.6000%	4.5000%

which are shown in Fig. 9(a)–(h). The branches between buses 800 to 816 are considered as part of the main feeder trunk.

High impedance faults were applied to all buses so as to validate the proposed methodology for the identification of the faulted lateral branch. For each estimate the error is obtained using (12). The average of these errors and the maximum errors obtained from the estimates are presented in Table 2. In this table, the first column describes the bus where the fault was applied, the second column contains the distance of this bus from the substation bus (SB), column 3 describes if the fault is at the main feeder trunk or in a lateral branch, column 4 informs if the method determined the correct faulted branch, column 5 presents the equivalent circuits indicated as containing the fault. Finally, columns 6 and 7 present the average and maximum errors obtained applying single line to ground faults at each phase of each bus.

From Table 2, it is verified that the average errors increase as the distance of the faulted bus from the substation bus increases. Nevertheless, the results were satisfactory, with average errors not exceeding 1.95%. For faults at buses within 30 km from the SB the average errors did not exceed 1.0%. Note that for faults at the buses 826, 828, 840, 842, 844 and 862 the methodology indicated two possible fault locations. Two possible fault locations can be determined for faults occuring close to buses where two lateral branches are connected and equivalent impedances of the equivalent circuits are similar. For instance, regarding buses 826 (circuit B) and 828 (circuit D-H), as these buses are close to bus 824, in which two lateral branches are connected (circuits B and D-H), the method determined two possible fault locations.

Analyzing the maximum errors presented in Table 2, it is also possible to conclude that the results were satisfactory, as the maximum errors did not exceed 4.021%. Note that the estimates are obtained for the entire set of samples after the fault is detected, thus considering the HIF build-up and shoulder periods. This explains the difference between maximum and average errors, since the transients introduced by the variation of the fault impedance may cause higher errors in the estimates.

To illustrate the proposed method for section identification, consider a fault at the bus 806 (main feeder trunk). The behavior of the sets of estimates, the fitted line equations and the corresponding R^2 values for the equivalent circuit are presented in Fig. 10. The eight equivalent circuits presented R^2 values with an absolute difference lower than 0.1, which indicates the fault in the main feeder trunk at 1.313 km from the substation bus. The R^2 values for all equivalent circuits are presented and discussed in Section 4.3.

The behavior of the estimates, the fitted line equations and corresponding \mathbb{R}^2 values for a fault at the bus 818 on phase A are presented in Fig. 11. This bus is part of the equivalent circuit A. According to Fig. 11, a lower \mathbb{R}^2 in circuit A compared to the other circuits is observed. Then, the proposed method correctly identified this fault as

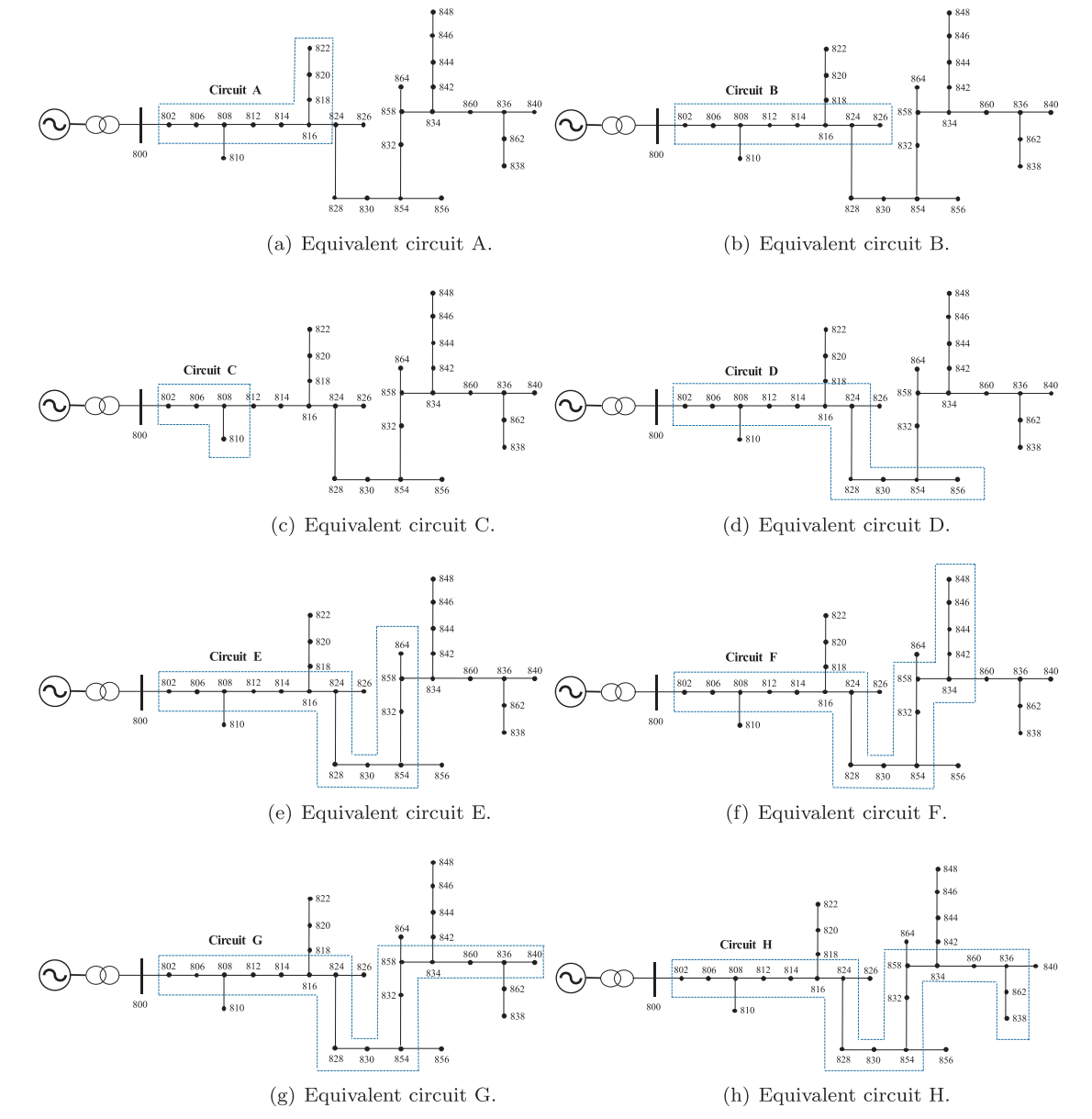


Fig. 9. Distribution system with lateral branches and equivalent systems.

belonging to circuit A. Circuits B and D-H presented the same behavior, which is reasonable since these circuits are equal from bus 800 to 824 and the fault was located upstream of bus 824. For circuit C, it is possible to observe a higher R^2 value when compared to the R^2 of circuit A, since it does not contain the fault.

Fig. 12 presents the behavior of the estimates, the fitted line equations and R^2 values for a fault at the bus 816. This bus is part of the equivalent circuits A, B and D-H, and is defined as part of the main feeder trunk. From Fig. 12, it is possible to verify similar R^2 values for these circuits. On the other hand, circuit C presented a higher R^2 value, since it does not contain the fault.

Considering a HIF at the bus 824 the method correctly determined the fault in circuits B and D-H. This result can be observed in Fig. 13, where the fitted lines and R^2 values for the equivalent circuits are presented. Circuit C presented a higher R^2 , since the fault is not located on it. Note that the R^2 values for circuits B and D-H are equal, and a higher R^2 is obtained in circuit A. As expected, the difference between the R^2 value of circuit A and the R^2 values of circuits B and D-H is higher than 0.1, since circuit A does not contain the fault.

The fitted line equations and corresponding R^2 values for a HIF at

the bus 826 (circuit B) is presented in Fig. 14. Once again, in circuit C a higher \mathbb{R}^2 value resulted, since the fault is not located in this circuit. In this case, the method determined two possible fault locations, in circuits B and D-H, when only circuit B contains the fault. This can be explained by the proximity of the bus 826 to bus 824, where two lateral branches (circuits B and D-H) are connected.

The fitted line equations and corresponding R^2 values for a fault at the bus 828 (circuit D-H) are presented in Fig. 15. The method determined two possible fault locations, in circuits B and D-H, when only circuits D-H contain the fault. This can be explained by the proximity to bus 824.

4.3. Analysis of tolerance in the difference between R² values

The faulted section identification, as presented in Section 3.3, is based on the analysis of the R^2 values and the definition of a tolerance in the difference between the R^2 values for each equivalent circuit. In order to demonstrate the empirical method to define this tolerance, consider the R^2 values presented in Table 3, which were obtained for faults in the main feeder trunk, for all equivalent circuits of the 34-bus

Table 2
Average and maximum errors.

Bus	km from SB	Fault at	Section determination	Equivalent circuit	μ Average	μ Maximum
802	0.786	Trunk	Correct	A - H	0.016%	0.047%
806	1.313	Trunk	Correct	A - H	0.011%	0.030%
808	11.136	Trunk	Correct	A - H	0.287%	0.577%
810	12.905	Lateral C	Correct	С	0.401%	1.024%
812	22.566	Trunk	Correct	A,B,D - H	0.886%	1.679%
814	31.627	Trunk	Correct	A,B,D - H	0.814%	1.488%
816	31.721	Trunk	Correct	A,B,D - H	0.816%	1.493%
818	32.242	Lateral A	Correct	A	0.927%	1.816%
820	46.918	Lateral A	Correct	A	1.186%	2.212%
822	51.106	Lateral A	Correct	A	1.453%	2.691%
824	34.833	Lateral B and D - H	Correct	B,D - H	0.793%	1.392%
826	35.756	Lateral B	2 locations	B,D - H	0.735%	1.676%
828	35.089	Lateral D - H	2 locations	D - H,B	0.712%	1.256%
830	41.319	Lateral D - H	Correct	D - H	0.986%	1.783%
832	52.697	Lateral E - H	Correct	E - H	1.631%	2.976%
834	55.957	Lateral F - H	Correct	F - H	1.873%	3.439%
836	57.377	Lateral G and H	Correct	G,H	1.885%	3.526%
838	58.957	Lateral H	Correct	H	1.947%	3.668%
840	57.637	Lateral G	2 locations	G,H	1.896%	3.544%
842	56.057	Lateral F	2 locations	F,G - H	1.878%	3.450%
844	56.467	Lateral F	2 locations	F,G - H	1.896%	3.499%
846	57.577	Lateral F	Correct	F	1.867%	3.575%
848	57.737	Lateral F	Correct	F	1.902%	3.586%
854	41.477	Lateral D - H	Correct	D - H	0.995%	1.799%
856	48.587	Lateral D	Correct	D	1.340%	3.111%
858	54.187	Lateral E - H	Correct	E - H	1.735%	3.959%
860	56.567	Lateral G and H	Correct	G,H	1.872%	3.477%
862	57.477	Lateral H	2 locations	H,G	1.888%	3.532%
864	54.687	Lateral E	Correct	E	1.750%	4.021%

feeder. In this table, the first column describes the bus where the fault was applied, while columns 2–9 present the R^2 values obtained for each equivalent circuit. Finally, column 10 presents six times the standard deviation (6 σ), which covers approximately 99% of the possible values.

From Table 3, it is possible to observe that the maximum value for 6σ is equal to 0.077. Thus, considering the absolute difference between R^2 values lower than 0.1 is sufficient to infer that the fault is located in more than one equivalent circuit. This sensitivity test, performed through the simulation of faults in the main feeder trunk, can be applied to define the tolerance for different networks.

4.4. Effect of noise in measurements

In order to evaluate the impacts of noise in the measurements, simulations considering a fault at the bus 808 were considered. For the voltage signal, it was applied a white gaussian noise considering an error of 1%. For the current signal, it was applied a white gaussian noise of 2%. Test results are presented in Table 4, where it is possible to observe a good performance of the presented method in the presence of noise.

5. Conclusion

This paper presented a physics-based analytical model for HIF location and section identification in PDS. The presented model is composed of two interdependent processes. First a frequency domain system model is used for fault location estimation. Considering a feeder with lateral branches, multiple fault location estimates are though obtained. In order to address this problem and determine the correct fault location, a methodology based on the analysis of the statistical behavior of the estimates is proposed, which is a contribution of this paper.

To validate the proposed formulation, several tests were carried out considering the IEEE 13-bus test feeder and a modified version of the IEEE 34-bus test feeder. A comparison with other state-of-the-art methods was presented, in which lower errors were obtained with the presented method for most of the cases.

The analytical method to solve the multiple estimates problem correctly identified the faulted section in great majority of test cases. In six cases two possible fault locations were determined, which was explained by the proximity of the faulted buses with a bus where two lateral branches are connected. The behavior of the R^2 obtained through linear regression of the estimates has demonstrated to be a good criterion to determine the faulted section. Furthermore, the average errors did not exceed 1.95%, thus demonstrating the potential application of the proposed method for real life applications. Further development of the model presented in this paper is currently being conducted to consider meshed distribution networks.

CRediT authorship contribution statement

Maicon J.S. Ramos: Conceptualization, Investigation, Methodology, Software, Validation, Writing - original draft. Mariana Resener: Resources, Writing - original draft, Writing - review & editing. Arturo S. Bretas: Supervision, Investigation, Writing - review & editing. Daniel P. Bernardon: Validation. Roberto C. Leborgne: Validation, Funding acquisition.

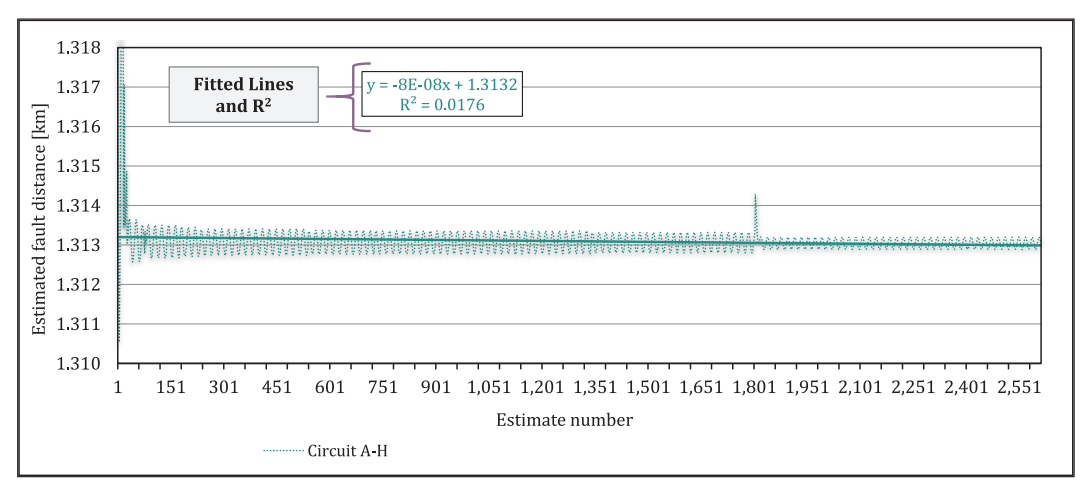


Fig. 10. Statistics of the sets of solutions considering a HIF on phase A at the bus 806 (main feeder trunk).

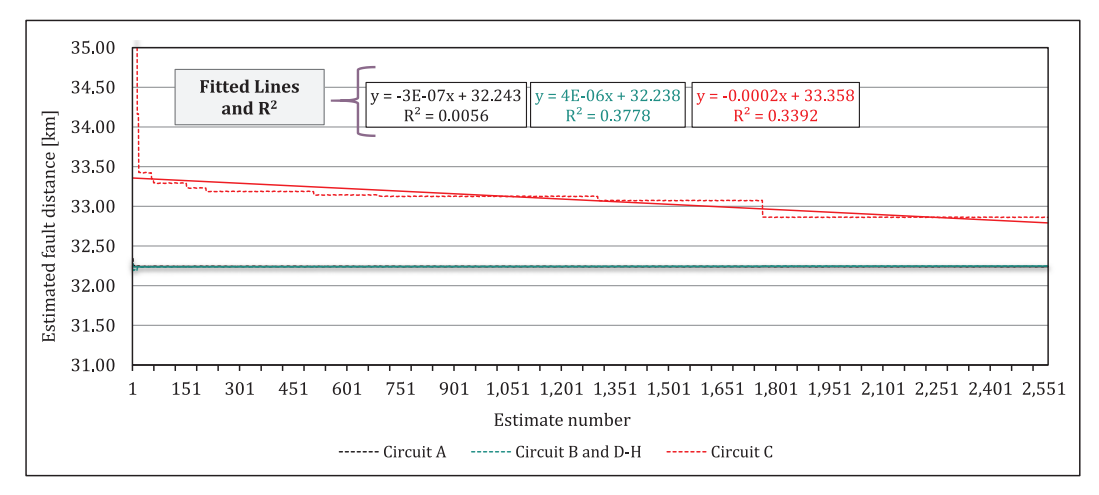


Fig. 11. Statistics of the sets of solutions considering a HIF at the bus 818 (circuit A).

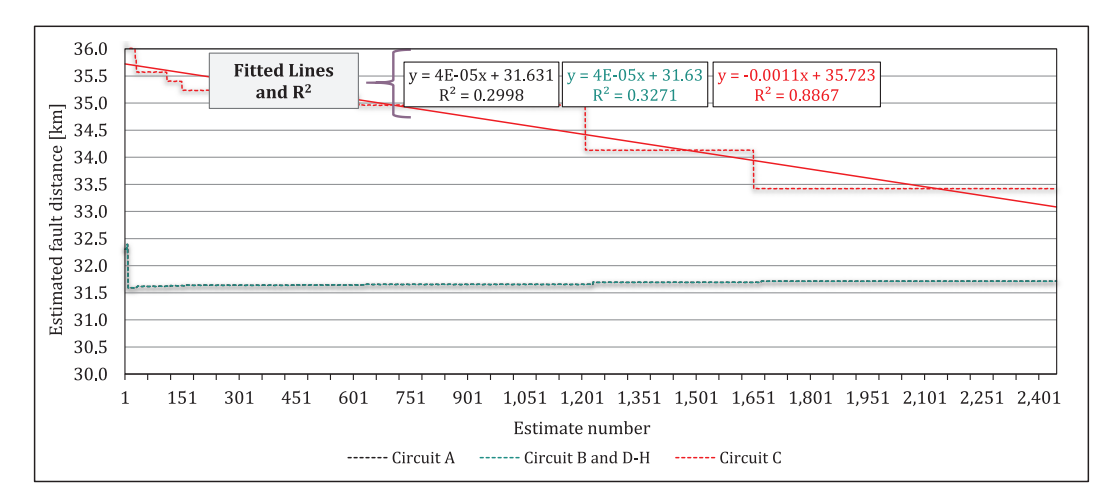


Fig. 12. Statistics of the sets of solutions considering a HIF at the bus 816 (main feeder trunk).

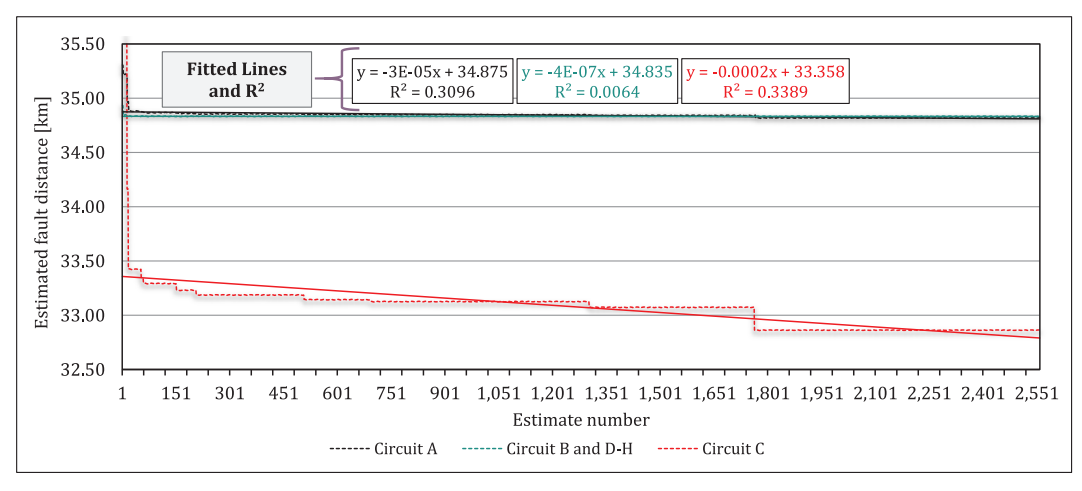


Fig. 13. Sets of solutions considering a HIF at the bus 824 (circuit B and D-H).

Declaration of Competing Interest

The authors declare that they have no known competing financial interests or personal relationships that could have appeared to influence the work reported in this paper.

Acknowledgment

This work was conducted during a Post Doctoral scholarship supported by the National Council for Scientific and Technological Development (CNPq) at the Federal University of Rio Grande do Sul - Brazil, grant 154750/2018-2.

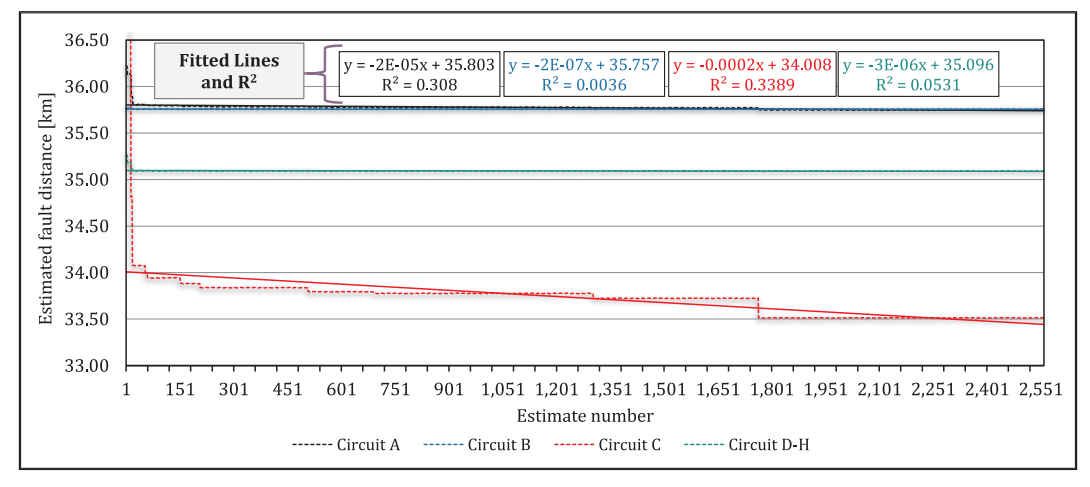


Fig. 14. Statistics of the sets of solutions considering a HIF at the bus 826 (circuit B).

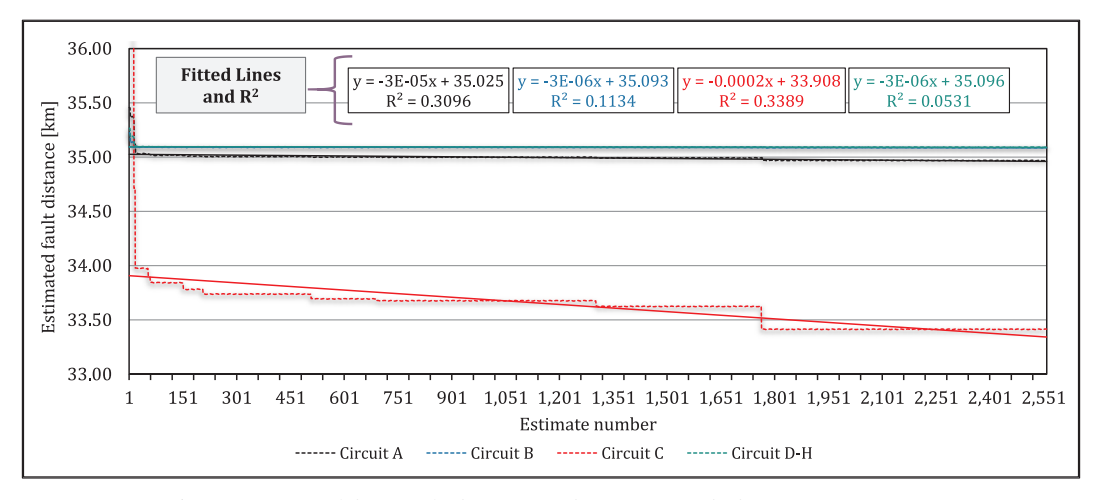


Fig. 15. Statistics of the sets of solutions considering a HIF at the bus 828 (circuits D-H).

Table 3 R^2 values for faults in the main feeder trunk.

	A	В	С	D	Е	F	G	Н	6σ
802	0.0174	0.0186	0.0172	0.0188	0.0176	0.0180	0.0192	0.0176	0.0044
806	0.0176	0.0189	0.0180	0.0195	0.0185	0.0181	0.0182	0.0193	0.0040
808	0.0055	0.0072	0.0035	0.0063	0.0060	0.0074	0.0066	0.0068	0.0075
812	0.0059	0.0067	-	0.0062	0.0064	0.0076	0.0071	0.0059	0.0038
814	0.0056	0.0058	-	0.0065	0.0074	0.0057	0.0059	0.0060	0.0038
816	0.2999	0.3271	-	0.3277	0.3321	0.3310	0.3387	0.3356	0.0770

Table 4Results considering noise - fault at the bus 808.

	Average error μ [ABC]	Maximum error μ [ABC]
With noise	0.340%	1.272%

References

- J.L. Blackburn, T.J. Domin, Protective Relaying: Principles and Applications, 4th ed., CRC press, 2015.
- [2] S. Jamali, N. Ghaffarzadeh, A new method for arcing fault location using discrete wavelet transform and wavelet networks, Eur. Trans. Electr. Power 22 (5) (2012) 601–615.
- [3] Z. Radojevic, J.-R. Shin, New one terminal digital algorithm for adaptive reclosing and fault distance calculation on transmission lines, IEEE Trans. Power Deliv. 21 (3) (2006) 1231–1237.
- [4] D. Jeerings, J.R. Linders, Ground resistance-revisited, IEEE Trans. Power Deliv. 4 (2) (1989) 949–956.

- [5] A. Emanuel, D. Cyganski, J. Orr, S. Shiller, E. Gulachenski, High impedance fault arcing on sandy soil in 15 kv distribution feeders: contributions to the evaluation of the low frequency spectrum, IEEE Trans. Power Deliv. 5 (2) (1990) 676–686.
- [6] R.H. Salim, M. Resener, A.D. Filomena, K.C.O. Rezende, A.S. Bretas, Extended fault-location formulation for power distribution systems, IEEE Trans. Power Deliv. 24 (2) (2009) 508–516.
- [7] A.D. Filomena, M. Resener, R.H. Salim, A.S. Bretas, Fault location for underground distribution feeders: an extended impedance-based formulation with capacitive current compensation, Int. J. Electr. Power Energy Syst. 31 (9) (2009) 489–496.
- [8] R.H. Salim, K.C.O. Salim, A.S. Bretas, Further improvements on impedance-based fault location for power distribution systems, IET Gener. Transm. Distrib. 5 (4) (2011) 467–478.
- [9] D.S. Gazzana, G.D. Ferreira, A.S. Bretas, A.L. Bettiol, A. Carniato, L.F.N. Passos, A.H. Ferreira, J.E.M. Silva, An integrated technique for fault location and section identification in distribution systems, Electr. Power Syst. Res. 115 (2014) 65–73.
- [10] R. Dashti, J. Sadeh, Fault section estimation in power distribution network using impedance-based fault distance calculation and frequency spectrum analysis, IET Gener. Trans. Distrib. 8 (8) (2014) 1406–1417.
- [11] R.G. Ferraz, L.U. Iurinic, A.D. Filomena, D.S. Gazzana, A.S. Bretas, Arc fault location: a nonlinear time varying fault model and frequency domain parameter estimation approach, Int. J. Electr. Power Energy Syst. 80 (2016) 347–355.

- [12] F. Aboshady, D. Thomas, M. Sumner, A new single end wideband impedance based fault location scheme for distribution systems, Electr. Power Syst. Res. 173 (2019) 263–270.
- [13] A. Johns, R. Aggarwal, Y. Song, Improved techniques for modelling fault arcs an faulted EHV transmission systems, IEE Proc.-Gener. Trans. Distrib. 141 (2) (1994) 148–154.
- [14] Z. Radojevic, V. Terzija, N. Djuric, Numerical algorithm for overhead lines arcing faults detection and distance and directional protection, IEEE Trans. Power Deliv. 15 (1) (2000) 31–37.
- [15] Z. Radojevic, H. Koglin, V. Terzija, A novel approach to the distance protection, fault location and arcing faults recognition, Power Systems Conference and Exposition, 2004. IEEE PES, vol. 2, (2004), pp. 628–634.
- [16] A. Bakar, M. Ali, C. Tan, H. Mokhlis, H. Arof, H. Illias, High impedance fault location in 11kV underground distribution systems using wavelet transforms, Int. J. Electr. Power Energy Syst. 55 (2014) 723–730.
- [17] L.U. Iurinic, R.G. Ferraz, A.S. Bretas, A.L. Bettiol, L.F.N. dos Passos, A. Carniato, I.K. Khairalla, R.Z. Homma, A. Baader, Fault induced transient detection in power systems: an adaptive approach considering noisy environment, International Conference on Power Systems Transients 2015 (IPST 2015), (2015).
- [18] A. Soheili, J. Sadeh, R. Bakhshi, Modified FFT based high impedance fault detection technique considering distribution non-linear loads: simulation and experimental data analysis, Int. J. Electr. Power Energy Syst. 94 (2018) 124–140.
- [19] L.U. Iurinic, A.R. Herrera-Orozco, R.G. Ferraz, A.S. Bretas, Distribution systems high-impedance fault location: aparameter estimation approach, IEEE Trans. Power Deliv. 31 (4) (2016) 1806–1814.
- [20] M.J. Ramos, A.S. Bretas, D.P. Bernardon, L.L. Pfitscher, Distribution networks HIF location: afrequency domain system model and WLS parameter estimation approach, Electr. Power Syst. Res. 146 (2017) 170–176.
- [21] P.E. Farias, A.P. de Morais, J.P. Rossini, G. Cardoso, Non-linear high impedance

- fault distance estimation in power distribution systems: a continually online-trained neural network approach, Electr. Power Syst. Res. 157 (2018) 20–28.
- [22] J. Nunes, A. Bretas, N. Bretas, A. Herrera-Orozco, L. Iurinic, Distribution systems high impedance fault location: aspectral domain model considering parametric error processing, Int. J. Electr. Power Energy Syst. 109 (2019) 227–241.
- [23] Z.M. Radojevic, A new spectral domain approach to the distance protection, fault location and arcing faults recognition on transmission lines, Int. J. Electr. Power Energy Syst. 29 (2) (2007) 183–190.
- [24] W.H. Kersting, Distribution System Modeling and Analysis, CRC press, 2012.
- [25] A. Monticelli, State Estimation in Electric Power Systems: A Generalized Approach, Springer Science & Business Media, 1999.
- [26] N.G. Bretas, A.S. Bretas, A two steps procedure in state estimation gross error detection, identification, and correction, Int. J. Electr. PowerEnergy Syst. 73 (2015) 484, 400
- [27] Y.-H. Lin, C.-W. Liu, A new DFT-based phasor computation algorithm for transmission line digital protection, Transmission and Distribution Conference and Exhibition 2002: Asia Pacific. IEEE/PES, vol. 3, (2002), pp. 1733–1737.
- [28] D.C. Montgomery, G.C. Runger, Applied Statistics and Probability for Engineers, John Wiley and Sons, Inc., 2014.
- [29] A.S. Bretas, N.G. Bretas, B.E. Carvalho, Further contributions to smart grids cyber-physical security as a malicious data attack: proof and properties of the parameter error spreading out to the measurements and a relaxed correction model, Int. J. Electr. Power Energy Syst. 104 (2019) 43–51.
- [30] W.H. Kersting, Radial distribution test feeders, IEEE Trans. Power Syst. 6 (3) (1991) 975–985.
- [31] A.G. Phadke, J.S. Thorp, Computer Relaying for Power Systems, John Wiley & Sons,
- [32] R.C. Dugan, M.F. McGranaghan, S. Santoso, H.W. Beaty, Electrical Power Systems Quality, McGraw-Hill, New York, USA, 2012.